

# DEM Modeling of Insertion and Expansion during Flat Dilatometer Testing

Tianlong Xu

Georgia Institute of Technology, Atlanta, USA. E-mail: [tianlong.xu@gatech.edu](mailto:tianlong.xu@gatech.edu)

J. David Frost

Georgia Institute of Technology, Atlanta, USA. E-mail: [david.frost@ce.gatech.edu](mailto:david.frost@ce.gatech.edu)

*Keywords:* Insertion effect, expansion effect, DEM modeling, flat dilatometer test, measure zones

**ABSTRACT:** This paper presents the results of a study that used the Discrete Element Method to model the insertion and expansion phases of the Flat Dilatometer Test (DMT) in sand. The dilatometer's size, penetration velocity, and membrane expansion were selected according to the ASTM standard test procedure. Sandy soil with zero water content were simulated with randomly generated circular particles, whose sizes are within a predefined range. The stress and strain rate histories in 15 sub-zones adjacent to the dilatometer's penetration path from top to bottom of the model chamber were determined and plotted as a function of the penetration stage. Parametric studies of lateral stress and soil density were conducted with three different models. Contact forces between the particles as well as the sensed forces of the device were also measured throughout the simulations. The results show that both the insertion and expansion phases of the DMT, although they behave in complex and different manners, have critical effects on the stress and strain changes in the soil.

## 1 INTRODUCTION

The Flat Dilatometer Test (DMT), invented by Dr. Silvano Marchetti in 1975, is an in-situ test device that uses pressure readings from the expansion of a circular membrane on the face of an inserted plate to interpret stratigraphy and provide estimates of at-rest lateral stress, elastic modulus, soil material classification index and shear strength of sands, silts, and clays.

Each simulated test consists of a vertical increment of penetration, followed by the expansion of a flat, circular, metallic membrane into the surrounding soil. Both the penetration and expansion phases of the test can cause disturbances to the soil, which changes the original condition of the undisturbed natural soil. Therefore the sensed data may require careful interpretation to evaluate the soil properties without the influence of these two effects.

This paper focuses primarily on the evaluation of the dilatometer's insertion and expansion. The paper presents a simulation of DMT progression with the Discrete Element Method program: PFC<sup>2D</sup>. In the study, particle sizes similar to sand grains were selected to conduct the simulations and different variables such as lateral

stress, and density were considered in the parametric study. During the modeling process, stress and strain rate changes in influenced zones as well as contact forces (both between soil particles and at soil-dilatometer interfaces) were recorded and analyzed. Sensed and influenced soil and dilatometer responses were also compared.

## 2 PREVIOUS LITERATURE REVIEW

Very limited documentation is available concerning the insertion and expansion effects of the DMT. However the literature cited herein does provide some useful insights.

Interactions between DMT blades and wet soils were studied by Campanella and Robertson in 1991. Their primary approach used a specially designed research-DMT to monitor device insertion effects in terms of pore pressure, membrane deflection and friction. Some of their conclusions are:

- 1) The strains (See Fig. 1) are quite large around the expanding membrane of a dilatometer but the expansion zone is probably still dominated by disturbed sand due to blade insertion;

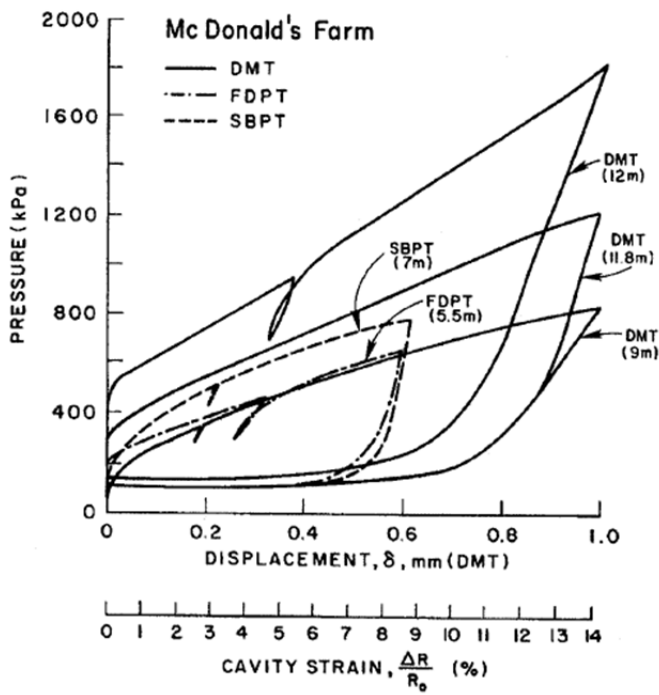


Fig. 1. Comparison of Research DMT and Pressuremeter Test Results in Sand (after Campanella, et al. 1991).

- 2) The slope of the DMT expansion curve shows a measure of the “elastic-plastic” response of sand;
- 3) The verticality of the blade can influence the friction while penetrating, and if the blade is deflected the friction along the deflected pushrod can be very large;

An Instrumented Dilatometer (IDMT) was also developed (Benoit et al. 2003) to record the continuous displacement of membrane, total pressure, and pore water pressure. A sensor located 60.7mm from the membrane center was integrated in this device to monitor the pore water pressure fluctuations. This approach showed that the pore water pressure increased during each IDMT insertion and that it started to decrease before the beginning of membrane expansion.

DMT effects were also studied through FEM modeling using PLAXIS code (Balachowski, 2006). The author compared the measured A and B values with calculated mean normal stress acting on the dilatometer after the blade insertion and after the inflation of the membrane, respectively. Parameters for the soil such as soil modulus, internal friction and dilatancy angle were considered in this approach. Figs. 2 and 3 illustrate several conclusions of this study. One important note is that the inflated membrane shape is not symmetric (Fig. 2) due to the stress distribution influence at the end of the insertion phase.

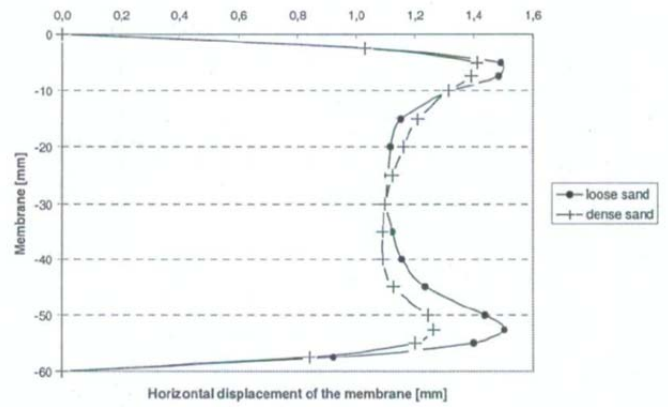


Fig. 2. The Shape of Inflated Membrane in Loose and Dense Sands (after Balachowski, 2006).

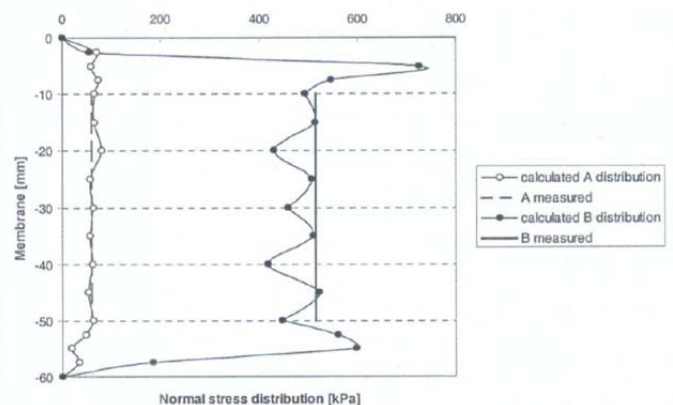


Fig. 3. Normal Stress Distribution for A and B Measurements in Loose Sand, calculation vs. experiment (after Balachowski, 2006).

This paper also noted that the boundary effect, which is a function of the diameter of the test chamber, can influence the result significantly.

Accordingly, the papers reviewed provided valuable insights for the study presented herein: first, it is critical to consider the soil model’s response in stress and strain in PFC<sup>2D</sup> under both insertion and expansion of DMT model and second, the responses of soil are also related to soil properties (density, friction and boundary conditions, amongst others).

### 3 BASIC SETTINGS

#### 3.1 Design of simulation devices

The simulation is performed in a chamber (boundary of the chamber are made of walls of balls in PFC<sup>2D</sup>) containing fully consolidated sandy soil particles. The dilatometer and membrane is made of shaped walls and their size and shape are designed to be similar to the device description in ASTM Standard 6635-01.

In order to simulate the two-phase membrane expansion process (membrane expansions to horizontal distances of 0.5 mm and 1.1 mm respectively, ASTM Standard 6635-01), a two-wall system (Fig. 4) was designed for use in the simulations. Key points are noted below:

- 1) The two walls move to the right alternatively;
- 2) The degrees of expansion are simulated quite well since the two arcs defining the walls have different curvatures;
- 3) The gradual and smooth transition of the two phases of membrane expansion is simulated reasonably well when the two walls cross each other and deviate apart.

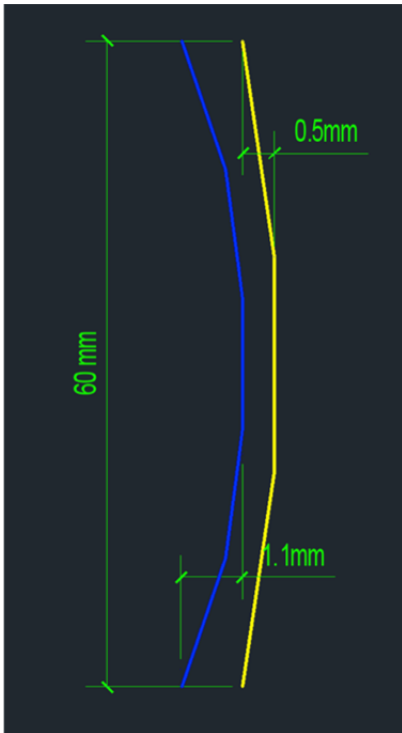


Fig. 4 Membrane expansion system

In summary, the dilatometer is a combination of three wall segments: the main body, the inner membrane and outer membrane.

### 3.2 Measure circles

In order to record the histories of stress and strain rate changes, ten measurement circles (1-10) are placed adjacent to the dilatometer's penetrating path on the right side of the blade and five similar measurement circles (11-15) are placed in the left side (Fig. 5). The center of the uppermost circle is located at a depth of 0.5 m while the distance between the measurement circles is 1 m. The radius of the circles is 0.1 m.

During the insertion and expansion simulation processes, interactions happen between walls and particles which causes stress changes and deformation of each measurement circle.

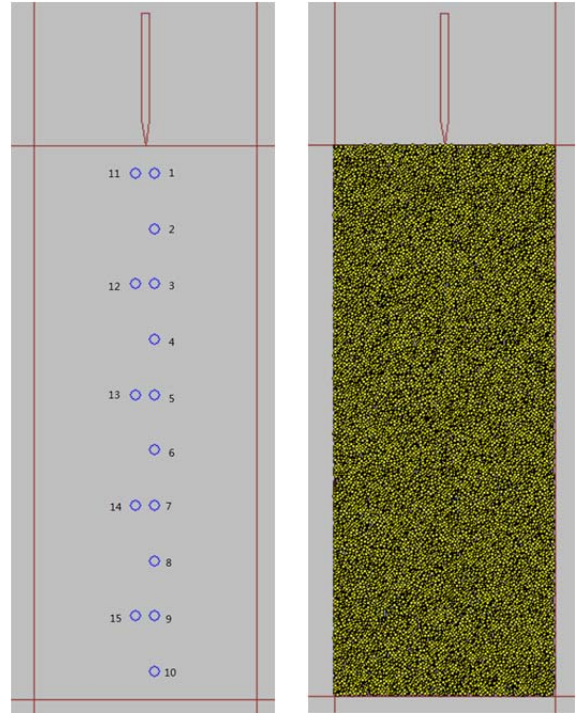


Fig. 5. Soil model and positions of measurement zones.

### 3.3 Simulation parameters

Basic model and simulation parameters for the various DEM models used in this study are summarized in Table 1.

Table 1. Basic parameters

Chamber size (meters, width×height)	4 × 10
Number of particles generated	19,995
Particle radius range (cm)	0.82~1.65
Average particle size (cm)	2.3
Porosity	0.18
Dilatometer thickness (cm)	15
Dilatometer height (cm)	240
Blade angle (°)	36
Membrane radius (cm)	30
Gravity (m/s <sup>2</sup> )	-9.81
Inter-particle friction coefficient ( <b>fric</b> in PFC <sup>2D</sup> )	0.4
Wall friction coefficient	0.0
Wall stiffness (N/m)	5 × 10 <sup>20</sup>
Particle stiffness (N/m)	5 × 10 <sup>8</sup>

In order to improve the performance and efficiency of computing, we used average particle size of 2.3 cm to perform all simulations, which is roughly 17 times more than the average size of coarse sand (size range 0.63~2 mm, ISO 14688-1). And the size of dilatometer is 10 times actual value.

In order to evaluate the effects of density and lateral stress, parametric studies for these two key variables were conducted. Six models were created for comparison (details are listed in Table 2).

Table 2. Parametric studies

Model	Density (kg/m <sup>3</sup> )	Lateral stress (Pa)
#1	1,500	Not controlled
#2	2,000	Not controlled
#3	2,500	Not controlled
#4	2,000	1×10 <sup>6</sup>
#5	2,000	2×10 <sup>6</sup>
#6	2,000	3×10 <sup>6</sup>

### 3.4 Simulation process

For each model, the complete simulation involved displacement of the dilatometer from the top to the bottom of the chamber, with the membranes expanding and contracting periodically during this process. To achieve this, three critical functions were created: insertion, expansion and contraction.

During the insertion phase, the dilatometer and its membranes are controlled to penetrate 1 m downwards along the center line of the chamber at a constant speed of 0.01 m/s. As a result of insertion, the particles adjacent to the dilatometer are displaced to either side as appropriate.

During the expansion phase, the dilatometer is maintained at the location where the insertion process was stopped. The inner membrane then starts to expand laterally, reaching a horizontal displacement of 0.5 mm and then stops; subsequently, the outer membrane starts to expand, reaching a horizontal displacement of 1.1 mm and then stops. During the contraction phase, the two membranes displace laterally back to the position where the expansion phase started. At that stage, the next insertion phase begins. The stress history and strain rate history of each measurement circle are all recorded and then extracted from PFC<sup>2D</sup> for analysis.

## 4 RESULT ANALYSIS

The results discussed in section 4.1, 4.2, and 4.3 are based on Model #2 in Table 2.

### 4.1 Contact forces

Under gravity of 9.81 m/s<sup>2</sup>, contact force is distributed evenly in the horizontal direction and it increases gradually in the vertical direction. As the dilatometer penetrates, the contact forces around the dilatometer increase (it can be seen that the contact forces around the dilatometer are much larger than in other areas, Fig. 6a) and the values of the contact forces further increase when the membrane is expanded (Fig. 6b). It decreases back to the conditions seen in Fig. 6a as the membrane contracts because of stress relaxation.

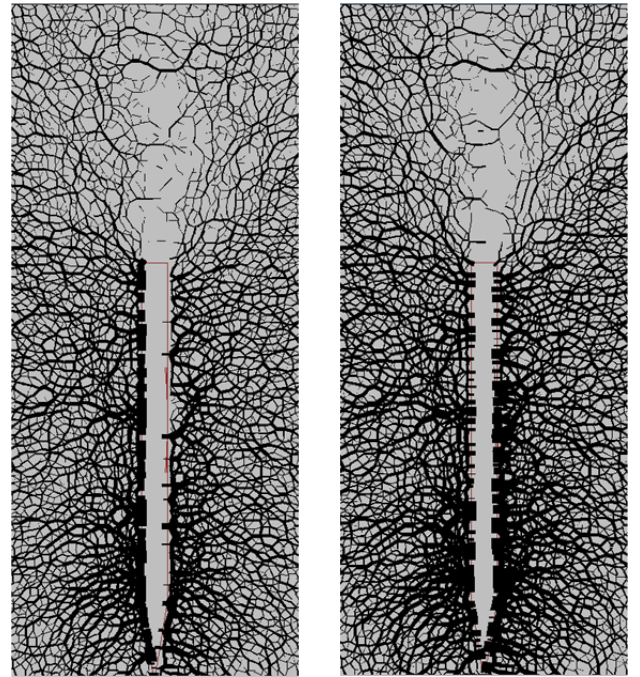


Fig. 6a. Insertion; Fig. 6b. Insertion plus Expansion.

### 4.2 Soil stress responses

Fig. 7 presents the soil stress responses for three measurement circles (circles 3, 5 and 7).

As the DMT approaches the measurement circles, the computed stresses in the circles start to change. For horizontal stress values, insertion and expansion both induce peak values, and the insertion effect is clearly evident. The peak values during insertion and expansion phases are roughly 5 and 3 times greater than the in-situ soil values, respectively.

Insertion also influences tangential stresses, with peak values appearing during the insertion phase and these peak values increase further when the dilatometer penetrates to a deeper location. Expansion effect is not so obvious in these plots and irregular stress distributions are observed when the dilatometer is moving beyond the measurement circle. This may be due to the redistribution of

particles after the state of stress has been disturbed by the instrument. For vertical stresses, insertion effects are obvious and the increase in stress is also approximately 5 times that of the pre-insertion in-situ stress value.

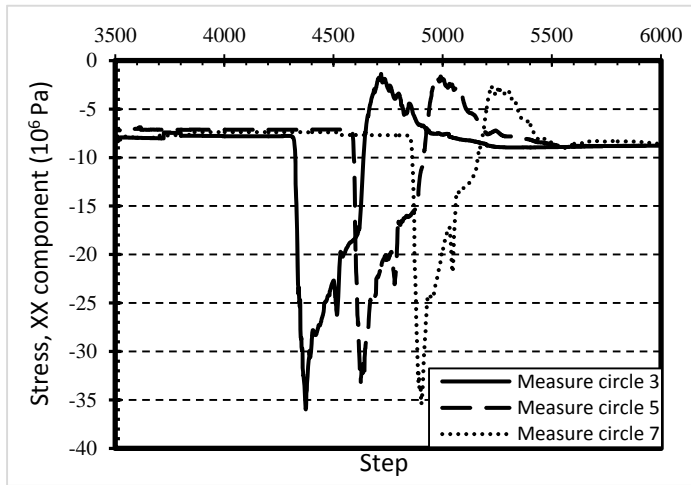


Fig. 7a. Stress history for  $\sigma_{11}$ .

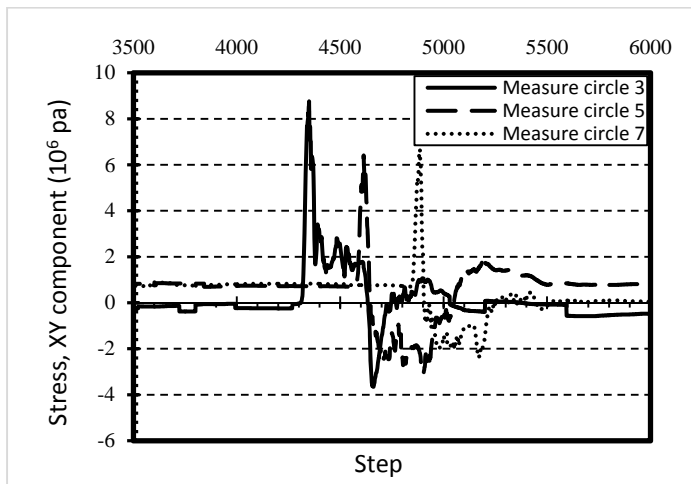


Fig. 7b. Stress history for  $\sigma_{12}$ .

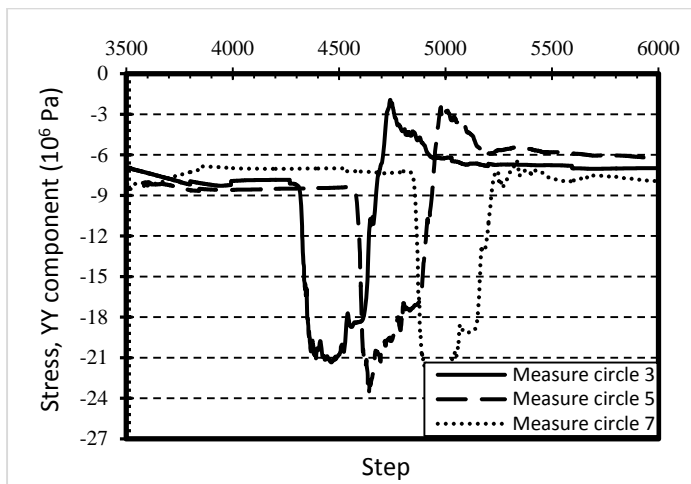


Fig. 7c. Stress history for  $\sigma_{22}$ .

In summary, insertion influences are more evident, especially on the horizontal stress in the soil. Expansion influences are observed in the horizontal stress plot albeit at a smaller magnitude.

### 4.3 Soil strain responses

Fig. 8 presents the soil strain rate responses for three measurement circles (circles 3, 5 and 7).

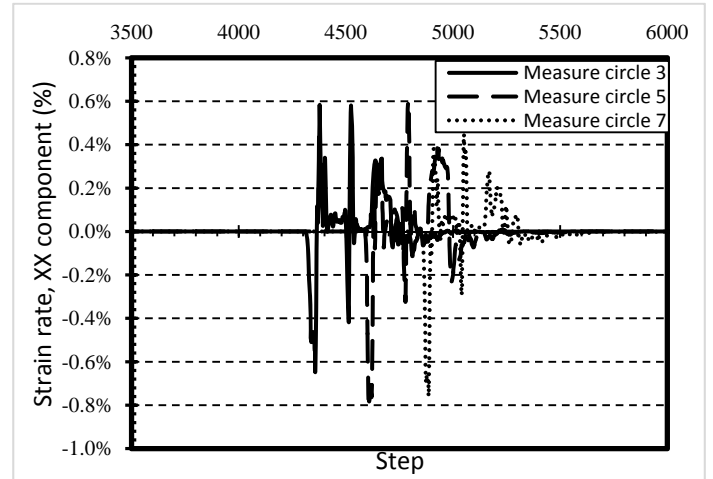


Fig. 8a. Strain rate history for  $\epsilon_{11}$ .

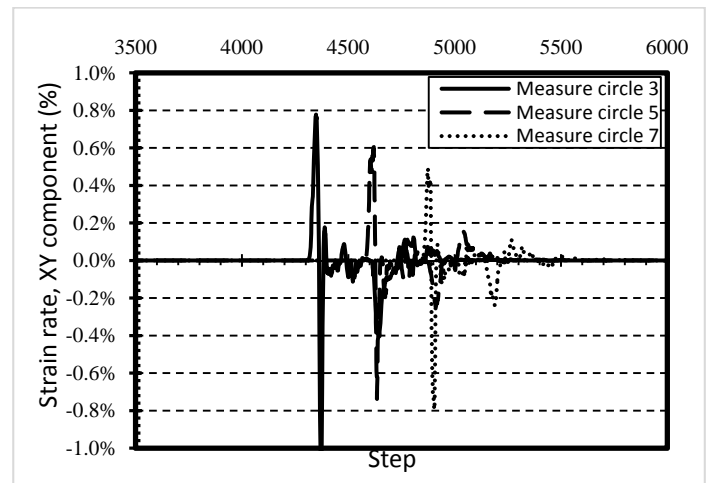


Fig. 8b. Strain rate history for  $\epsilon_{12}$ .

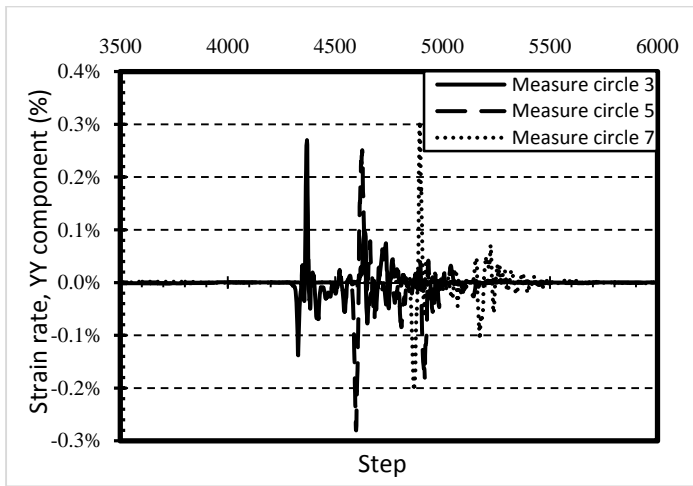


Fig. 8c. Strain rate history for  $\epsilon_{22}$ .

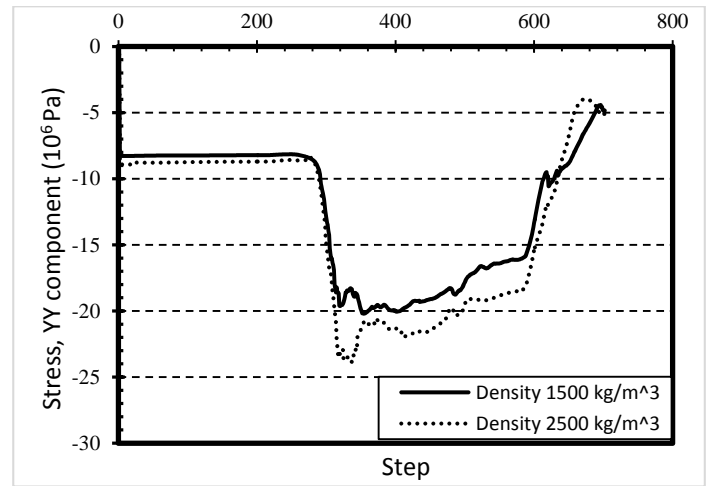


Fig. 9b. Stress history for  $\sigma_{22}$ .

Insertion effects also dominate in terms of strain rate. They cause horizontal strain rates to decrease first and then increase. For vertical strain, the increased magnitude is greater while for horizontal strain, the decreased magnitude is greater, which obeys compatibility law (Davis 2002). The influence of insertion on  $\epsilon_{11}$  and  $\epsilon_{12}$  (peak values of 0.6% and 0.8%, respectively) is greater than on  $\epsilon_{22}$  (peak value 0.28%).

Expansion effects are limited to horizontal strain rate and cause the measurement circles to contract in the horizontal direction and thus expand in the vertical direction. Volume change caused by expansion is smaller than insertion. However, its influence on horizontal strain rate is about half that observed for insertion. Irregular strain rate changes are observed for tangential strains during expansion.

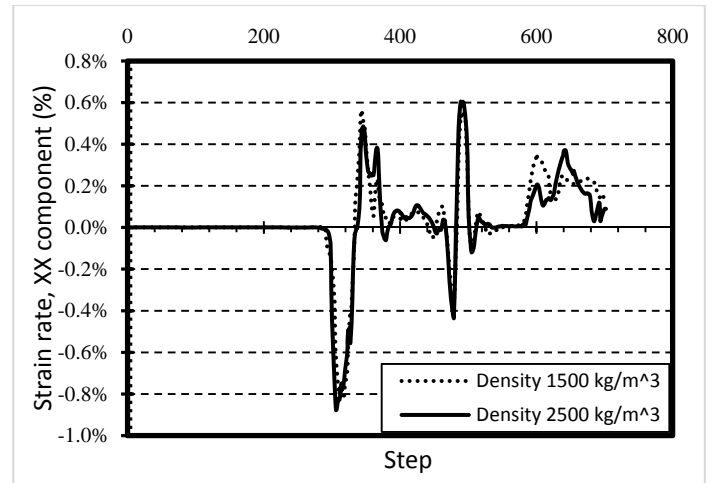


Fig. 10a. Strain rate history for  $\epsilon_{11}$ .

#### 4.4 Parametric study: density effect

Density plays a key role in influencing the interaction process between particles and dilatometer.

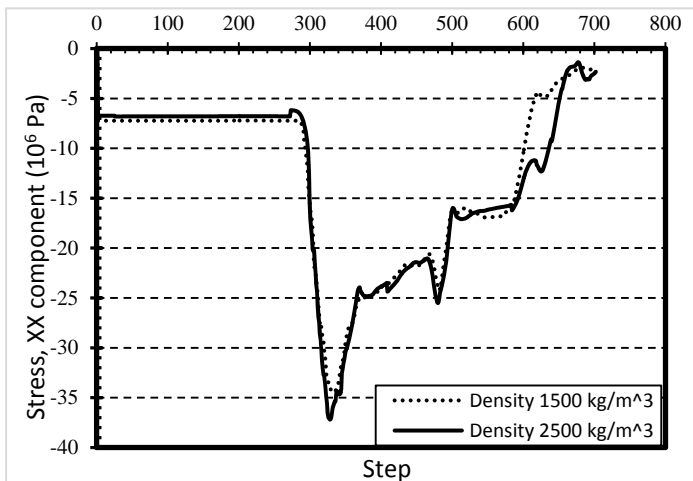


Fig. 9a. Stress history for  $\sigma_{11}$ .

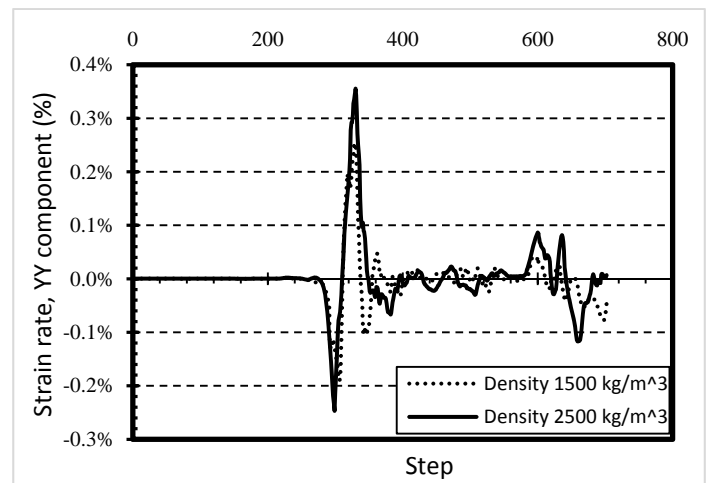


Fig. 10b. Strain rate history for  $\epsilon_{22}$ .

Models with different densities were created by changing the model settings in PFC<sup>2D</sup>. The effect of density can be illustrated by comparing results of model #1 and #3. Selected graphs for measurement circle 5 are shown in Fig. 9 and Fig. 10.

Fig. 9 and Fig. 10 show the results of horizontal and vertical components of stress and strain rate for two different densities. Comparing the results for these two densities, some differences can be noted. Stress influence caused by insertion is marginally greater for denser soil. Also, the denser sample shows a more direct response to strain rate change during the insertion process.

#### 4.5 Parametric study: lateral stress effect

In order to investigate the effect of lateral stress, servo-control simulation was performed in PFC<sup>2D</sup> to create boundary conditions reflective of different lateral stresses. As noted in Table 2, lateral stress at the boundary was controlled to be  $1 \times 10^6$ ,  $2 \times 10^6$  and  $3 \times 10^6$  Pa, respectively.

The effect of lateral stress can be illustrated by comparing the results of model #4 and model #6. Example plots for measurement circle 5 are shown in Fig. 11 and Fig. 12.

It can be seen that the dashed lines and solid lines have different starting points (Fig. 11), which represents the different boundary conditions in terms of lateral stress for the different models.

To be summed, Lateral stress, as a critical parameter, effects dilatometer-soil interaction in the following manner:

- 1) Higher lateral stress can mitigate the stress disturbance caused by dilatometer insertion and expansion effects.
- 2) Higher lateral stress results in smaller deformations caused by dilatometer insertion and expansion processes.
- 3) The dilatometer influences soil behavior more significantly in terms of vertical stress than horizontal stress.

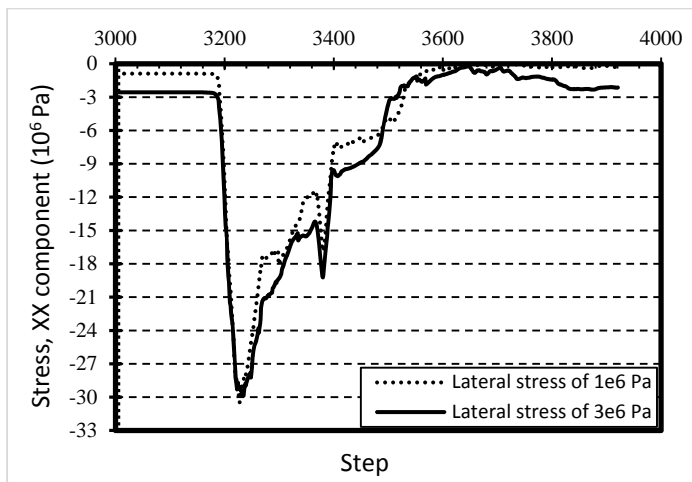


Fig. 11a. Stress history for  $\sigma_{11}$ .

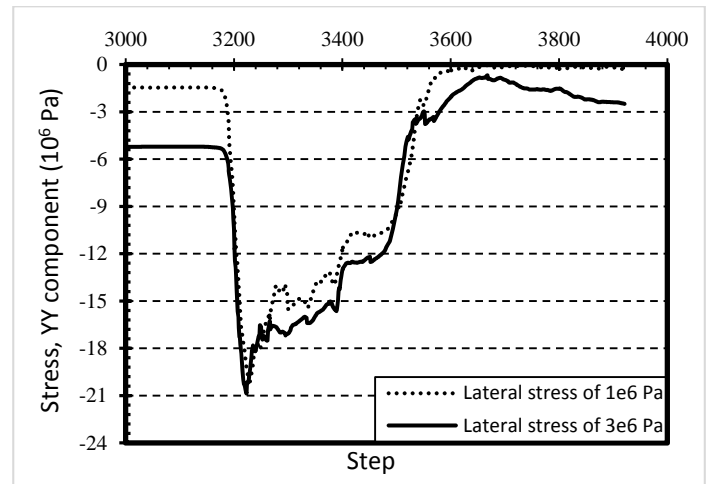


Fig. 11b. Stress history for  $\sigma_{22}$ .

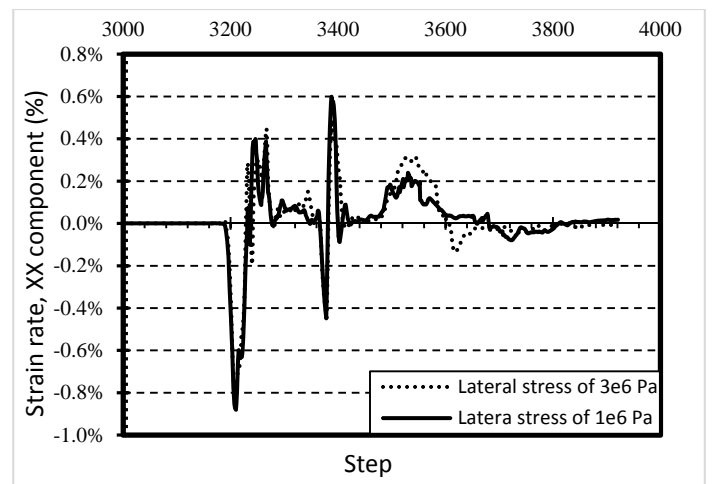


Fig. 12a. Strain rate history for  $\epsilon_{11}$ .

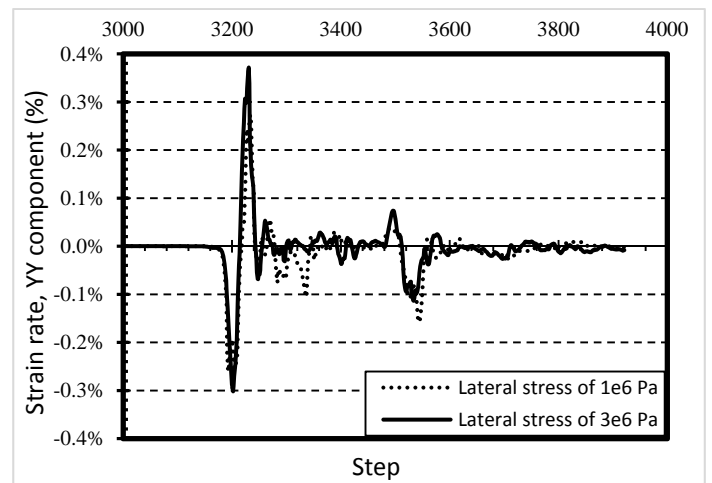


Fig. 12b. Strain rate history for  $\epsilon_{22}$ .

#### 4.6 Sensed forces by DMT components

Membrane sensed force and dilatometer sensed force are critical to study the interaction of the soil and the device. Fig. 13 and Fig. 14 presents some important results illustrating this.

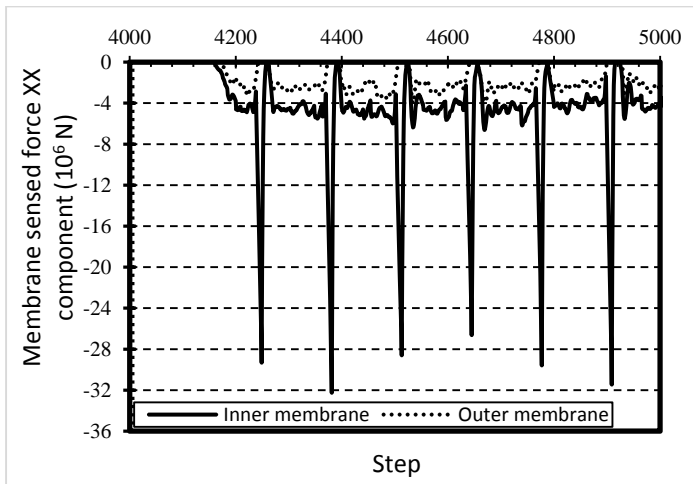


Fig. 13. X force sensed by membranes.

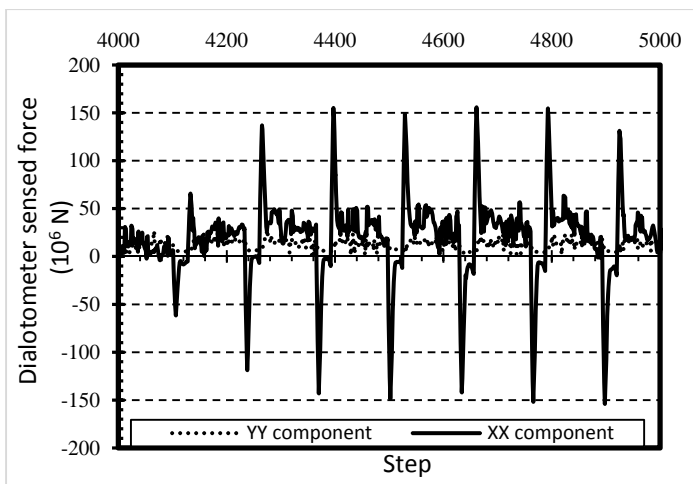


Fig. 14. X, Y force sensed by dilatometer.

In Fig. 13, it can be seen that the dashed line is totally within the envelope of the solid line. This means that the outer membrane sensed force in the horizontal direction is smaller than that of the inner membrane. This is mainly due to the redistribution of particles after the first phase of expansion.

With respect to the dilatometer sensed force, it appears that the force in the X direction is more prevalent (Fig. 14) and that the insertion effect is more dominant than the expansion effect.

## 5 CONCLUSIONS

In summary, a number of important observations related to DMT insertion and membrane expansion result from the DEM simulations presented herein:

- 1) The insertion and expansion processes of the dilatometer influence soil behavior by changing the state of stress and producing local deformations;

- 2) Insertion effects dominate and their influence has greater impact on horizontal stress than vertical stress;
- 3) Expansion effects mainly influences horizontal stress;
- 4) Insertion causes the soil to be laterally contracted initially and then extended; subsequent membrane expansion exacerbates this effect;
- 5) Denser soil behaves more visibly in terms of stress change while looser soil shows greater deformation during the DMT insertion stage;
- 6) Higher lateral stress can mitigate stress disturbance and produces smaller deformations.
- 7) When servo-control changes the boundary lateral stress, the local vertical stress is more impacted than the local horizontal stress is.

## 6 ACKNOWLEDGEMENTS

The authors would like to thank Sacha Emam and Derrick Blanksma in Itasca Inc. for the information they offered about DEM coding. Constructive suggestions from two PhD students, Alejandro Martinez and Jackson Su in School of Civil Engineering, Georgia Tech are also appreciated.

## 7 REFERENCE:

- Campanella, R. G., and Robertson, P.K. (1991). "Use and Interpretation of a Research Dilatometer." *Can. Geotech. J.*, **28**, 113-126.
- Benoit, J., and Stetson, K.P. (2003). "Use of an Instrumented Flat Dilatometer in Soft Varved Clay." *J. Geotech. Geoenviron. Eng.*, Vol. **129** (12), 1160-1167.
- Balachowski, L. (2006). "Numerical Modelling of DMT Test in Calibration Chamber." *Studia Geotechnica et Mechanica*, Vol. XXVIII, No. 2-4.
- Poulos, H.G., and Davis, E.H. (1974). "Elastic Solutions for Soil and Rock Mechanics." *Wiley and Sons*, New York.
- Davis, R.O. and Selvadurai, A.P.S. (2002). "Plasticity and Geomechanics." *Cambridge University Press*, New York.
- ASTM Standards: D 6635-01. (2007) "Standard Test Method for Performing the Flat Dilatometer Test." *ASTM C700*, West Conshohocken, PA.
- ISO Standards: ISO 14688-1. (2002) "Geotechnical investigation and testing -- Identification and classification of soil --Part 1: Identification and description."
- Mayne, P.W., Christopher, B.R. and DeJong, J. (2002). "Manual on Subsurface Investigations." *National Highway Institute. Federal Highway Administration*, Washington, DC. Page 5-16.
- Itasca, (2006). "Manual of PFC<sup>2D</sup> 3.10 (Particle Flow Code in Two Dimensions)." *Itasca Consulting Group, Inc.*, Minnesota.